American Mineralogist, Volume 65, pages 920–930, 1980

Structure and elastic properties of quartz at pressure

LOUISE LEVIEN[1], CHARLES T. PREWITT AND DONALD J. WEIDNER

Department of Earth and Space Sciences
State University of New York
Stony Brook, New York 11794

Abstract

Unit cells and crystal structures were determined on a single crystal of quartz at seven pressures from 1 atm to 61.4 kbar. Unit-cell parameters are $a = 4.916(1)$ and $c = 5.4054(4)$Å at 1 atm, and $a = 4.7022(3)$ and $c = 5.2561(2)$Å at 61.4 kbar. Structural changes observed over this pressure range include a decrease in the Si–O–Si angle from 143.73(7)° to 134.2(1)°, a decrease in the average Si–O bond distance from 1.6092(7) to 1.605(1)Å, and an increase in distortion of the silicate tetrahedron. Several O–O distances show very large changes (11%) that can be related to the unit-cell-edge compression. As pressure is increased, the geometry of the SiO_2 (quartz) structure approaches that of the low-pressure GeO_2 (quartz) structure.

The structural changes that take place with increased temperature are not the inverses of those that occur with increased pressure; changes in the Si–O–Si angle and the tetrahedral tilt angle control thermal expansion, whereas smaller changes in the Si–O–Si angle and tetrahedral distortion control isothermal compression.

By constraining the zero-pressure bulk modulus to be equal to that calculated from acoustic data [$K_T = 0.371(2)$ Mbar], the pressure derivative of the bulk modulus at zero pressure [$K'_T = 6.2(1)$] has been calculated by fitting the P–V data to a Birch-Murnaghan equation of state. The anomalously low value of Poisson's ratio in quartz can be explained by the low ratio of the off-diagonal shear moduli to the pure-shear moduli. This small ratio reflects the easily expanding or contracting spirals of tetrahedra that behave like coiled springs.

Introduction

The literature on the crystal structure and compressibility of quartz leaves many questions about its changes with pressure. As high-pressure structural refinements have not been as precise as those performed under ambient conditions, these studies report large changes (*e.g.,* the Si–O–Si interbond angle); however, subtle ones have not been previously resolvable. Recent experimental developments in our laboratory offer the potential of providing improved resolution in high-pressure structural data.

The crystal structure of quartz at room temperature and pressure has been refined many times (Young and Post, 1962; Smith and Alexander, 1963; Zachariasen and Plettinger, 1965; Le Page and Donnay, 1976; Jorgensen, 1978; d'Amour *et al.,* 1979), with the Young and Post and the Smith and Alexander papers reporting the first quality refinements of positional parameters and thermal ellipsoids. Zachariasen and Plettinger improved upon these studies by applying a secondary-extinction correction to their refinement. The Le Page and Donnay refinement again improved the R value; however, no corrections for crystal X-ray absorption or extinction were made. Both Jorgensen and d'Amour *et al.* collected intensity data for room-pressure structural refinements with crystals already loaded in high-pressure cells; these refinements are of lower precision than the others.

Static-compressibility studies on quartz were first carried out by Adams and Williamson (1923) and Bridgman (1925; 1928), and then greatly improved by Bridgman (1948a,b; 1949) and others (McWhan, 1967; Vaidya *et al.,* 1973; Olinger and Halleck, 1976; Jorgensen, 1978; d'Amour *et al.,* 1979). McWhan measured the compression of quartz in a modified Bridgman-anvil apparatus with Guinier geometry

[1] Present address: Division of Geological and Planetary Sciences, California Institute of Technology, Pasadena, California 91125.

0003–004X/80/0910–0920$02.00

X-ray cameras, using NaCl as both a pressure-transmitting medium and a calibration standard. The experiments were carried out to 150 kbar and no evidence of a phase transition was seen, despite the fact that the sample had been subjected to pressures higher than required to transform quartz to coesite and stishovite at high temperature. The Vaidya *et al.* compressibility data were collected in a piston–cylinder apparatus with indium, a low shear-strength metal, as the pressure-transmitting medium. Displacement of a piston was measured to determine the volume change; therefore, the data at low pressures, where voids are being closed, are not as accurate as the higher-pressure data. The Olinger and Halleck study was performed in a modified Bridgman-anvil apparatus, using a 4:1 methanol:ethanol mixture as the hydrostatic pressure-transmitting fluid. Jorgensen collected hydrostatic high-pressure neutron-diffraction data on a powdered sample, determining changes in both unit cell and crystal structure. The d'Amour *et al.* work, the only previous compressional study of quartz using single-crystal X-ray techniques, also gave unit-cell parameters and structural data.

Experimental techniques

A clear crystal of natural quartz was broken, and a platy fragment (70 μm × 50 μm × 30 μm) used for this study, with c approximately normal to the plane of the plate. Although precession and Weissenberg X-ray photographs showed the crystal to be of high quality, intensity data were collected on the crystal before it was loaded into the diamond cell. The refinement of these data were used both for comparison purposes and to check for Dauphiné twinning, which cannot be distinguished easily with film techniques because it is only recognizable as increased or decreased intensity of a certain class of reflections (Young and Post, 1962). We refined the structure both with the entire set of structure factors and with the structure factors not affected by Dauphiné twinning (*hhl* and *hk*0). Having found essentially identical refinements for these two sets of data, we decided not to make a correction for Dauphiné twinning of the sample. Room-pressure and 31-kbar data were collected with Ag$K\alpha$ radiation, which has two potential advantages over Mo$K\alpha$ radiation for diamond-cell work: its shorter wavelength makes more of the reciprocal lattice accessible, and its linear-absorption coefficients are smaller than those for Mo$K\alpha$. However, the lower intensity of the incident Ag$K\alpha$ radiation and the poorer counting efficiency of the scintillation detector more than offset the above advantages and make Ag$K\alpha$ less desirable. The refinement of the 31-kbar structure, collected with Ag$K\alpha$ radiation, resulted in R values three times those of the Mo$K\alpha$ data sets and has therefore been omitted from this report.

The quartz crystal was mounted in a Merrill-Bassett design single-crystal diamond-anvil cell (Merrill and Bassett, 1974). The diamonds (1/8 carat each) had 0.65 mm faces (culet), and the gasketing material [250 μm thick Inconel X750 (spring)] had a 300 μm hole. The crystal was attached to one diamond face with the alcohol-insoluble fraction of petroleum jelly, and a 4:1 methanol:ethanol mixture was used as the pressure-transmitting medium (Finger and King, 1978; Piermarini *et al.,* 1973). A small ruby crystal (10 μm; 0.5 wt.% Cr) (Piermarini *et al.,* 1975) in the cell was used for pressure calibration, which was performed both before and after X-ray data were collected. The pressure-calibration system, based on the shift of the fluorescence spectrum of ruby, is similar to that described by Barnett *et al.* (1973) but modified by King (1979). The diamond cell was then mounted on a specially designed goniometer head (Hazen and Finger, 1977; Finger and King, 1978), which was in turn mounted on a four-circle X-ray diffractometer. Both before and after intensity data were collected at each pressure, unit-cell parameters were determined, using King and Finger's (1979) method of avoiding systematic errors resulting from an uncentered crystal.

With the exception of the room-pressure determination, an entire sphere of integrated intensities in reciprocal space ($2° < 2\theta < 90°$) was collected with crystal-monochromatized Mo$K\alpha$ radiation; a hemisphere of intensities ($2° < 2\theta < 45°$) (Ag$K\alpha$) was collected on the crystal at room pressure. Intensities were measured using a quasi-constant-precision counting scheme with reflections less than $2\sigma_I$ considered unobserved; σ_F's were calculated by adding to the constant-precision value an additional factor that reflects the fluctuation of the incident beam (Baldwin and Prewitt, in preparation). Structure factors were corrected for X-ray absorption of the diamond cell (Finger and King, 1978) and crystal X-ray absorption. Several reflections with exceptionally high or asymmetrical background counts were rejected from each of the high-pressure data sets because of overlap with diamond reflections. None of the reflections with 2θ values near or on the 2θ values of beryllium metal were collected. Symmetrically equivalent reflections were averaged, yielding between 198 and

Table 1. Intensity information for quartz at six pressures

	Total # data	# after av.*	$\#>2\sigma_I$**	wR	R	Ext.x10^{-4}***	$\delta^\dagger$
1 atm	663	210	194	0.019	0.016	0.11(1)	-16.37
20.7(5)†† kbar	390	198	170	0.029	0.029	0.32(4)	-19.54
37.6(5) kbar	438	215	190	0.031	0.032	0.34(4)	-21.58
48.6(5) kbar	440	217	196	0.032	0.034	0.37(4)	-22.46
55.8(5) kbar	432	214	200	0.028	0.026	0.34(3)	-23.05
61.4(5) kbar	426	215	191	0.031	0.034	0.23(3)	-23.47

*Number of data after symmetrically equivalent reflections were averaged.
**Number of data accepted in the refinement. All were greater than $2\sigma_I$.
***Refined secondary extinction parameters.
†The tetrahedral tilt parameter from Grimm and Dorner (1975).
††Parenthesized figures represent esd's of least units cited.

218 independent reflections at each pressure. Anisotropic refinements of the structure were executed using the least-squares program RFINE4 with a $1/\sigma^2$ weighting scheme (Finger and Prince, 1975). In the high-pressure data sets, all observed reflections were accepted; two reflections were rejected from the room-pressure refinement. The final weighted R values range from 0.019 to 0.032 (Table 1). Observed and calculated structure factors are listed in Table 2[2]; positional parameters and temperature factors are reported in Table 3; interatomic distances and angles are given in Table 4; and unit-cell parameters are listed in Table 5.

Room-pressure structural study

The refined positional parameters, bond distances and angles of our room-pressure study (Tables 3 and 4) are in better agreement with the Zachariasen and Plettinger (1965) refinement than with the more recent refinement of Le Page and Donnay (1976). Le Page and Donnay suggest that the large discrepancy between their x and y oxygen parameters and those of Zachariasen and Plettinger may be due to the limited $\sin\theta/\lambda$ range of the latter study. Data for our room-pressure refinement were collected to a maximum $\sin\theta/\lambda$ of 0.68Å^{-1} and fall closer to the 0.64Å^{-1} Zachariasen and Plettinger value than to that of Le Page and Donnay (0.99Å^{-1}). Le Page and Donnay based their decision not to make a secondary extinction correction on a calculation derived from Zachariasen (1963). To determine the effect of extinction on a reflection, its transmission factor is required. Transmission factors are commonly determined during the crystal X-ray absorption correction, but no such correction was made by Le Page and Donnay because of the crystal's odd shape. Therefore, their calculation to determine the necessity of an extinction term must have been made assuming equal transmission factors for all reflections. This incorrect assumption may have biased their calculation, and therefore improperly suggested that no extinction term was necessary. In addition, this model tests only type I extinction, and Zachariasen (1967) showed that the quartz crystal he studied in 1965 suffers from type II extinction as well. The refinement of a secondary-extinction parameter for our data brought even the largest F_{obs} ($10\bar{1}$) (which was rejected in the two prior studies) into excellent agreement with its F_{calc} (Tables 1 and 2), and decreased the R values of all six of our refinements at the 0.005 significance level (Hamilton, 1974). The temperature factors in our 1 atm refinement are larger than in the other 1 atm refinements or our high-pressure refinements (performed with Mo$K\alpha$ radiation and over a larger $\sin\theta/\lambda$ range). The thermal ellipsoid for Si is nearly spherical, as shown by the approximately equal RMS amplitudes [0.085(1), 0.085(1), 0.095(1)] and the very large (~105°) errors on the angles that describe the thermal ellipsoid's orientation relative to the crystallographic axes.

Grimm and Dorner (1975) suggest that the α–β transition in quartz can be described as a simultaneous tilting of the tetrahedra around the twofold axes perpendicular to c. They derive the following equation to quantify the tilt angle, δ, in the quartz structure,

$$\tan\theta = \frac{2\sqrt{3}}{9}\,\frac{c}{a}\,\frac{6z-1}{x}$$

[2] To receive a copy of Table 2, order Document AM-80-140 from the Business Office, Mineralogical Society of America, 2000 Florida Avenue, N.W., Washington, D.C. 20009. Please remit $1.00 in advance for the microfiche.

Table 3. Positional and thermal parameters of quartz at pressure

	1 atm	20.7*	37.6	48.6	55.8	61.4
x(Si)	0.4697(1)**	0.4630(2)	0.4581(2)	0.4551(2)	0.4537(2)	0.4526(2)
x(O)	0.4135(3)	0.4111(6)	0.4079(6)	0.4061(6)	0.4047(5)	0.4034(6)
y(O)	0.2669(2)	0.2795(4)	0.2867(5)	0.2912(5)	0.2926(4)	0.2952(5)
z(O)	0.1191(2)	0.1095(2)	0.1039(3)	0.1012(3)	0.0998(2)	0.0987(3)
B(Si)	0.62(2)	0.44(2)	0.47(2)	0.51(2)	0.49(2)	0.49(2)
B(O)	1.05(2)	0.86(3)	0.88(3)	0.84(3)	0.80(2)	0.79(3)
β_{11}(Si)†	0.93(2)	0.70(4)	0.79(4)	0.87(4)	0.82(3)	0.84(4)
β_{22}(Si)	0.78(2)	0.57(5)	0.68(5)	0.70(5)	0.74(4)	0.69(5)
β_{33}(Si)	0.49(2)	0.35(2)	0.35(2)	0.39(2)	0.36(2)	0.39(2)
β_{13}(Si)	-0.001(7)	0.02(1)	-0.05(1)	-0.03(1)	-0.02(1)	-0.02(1)
β_{11}(O)	1.90(6)	1.48(9)	1.55(10)	1.50(10)	1.53(8)	1.48(10)
β_{22}(O)	1.44(5)	1.08(8)	1.23(9)	1.28(10)	1.17(7)	1.21(9)
β_{33}(O)	0.83(3)	0.76(3)	0.69(3)	0.65(3)	0.62(3)	0.64(3)
β_{12}(O)	1.06(5)	0.75(8)	0.75(10)	0.78(10)	0.79(8)	0.80(10)
β_{13}(O)	-0.25(3)	-0.34(6)	-0.40(6)	-0.42(6)	-0.32(4)	-0.27(6)
β_{23}(O)	-0.35(3)	-0.29(4)	-0.32(4)	-0.31(4)	-0.30(3)	-0.26(4)

Pressures reported in kbar unless otherwise stated.
**Parenthesized figures represent esd's of least units cited.*
†*All anisotropic temperature factors, β's, are given x 10^2.*
β_{12} *and* β_{23} *for Si are constrained to be 1/2* β_{22} *and 2* β_{13}*, respectively.*

Table 4. Selected interatomic distances and angles of quartz at pressure

	1 atm	20.7*	37.6	48.6	55.8	61.4
Intra-tetrahedral distances						
Si-O (Å)**	1.605(1)	1.604(2)	1.601(3)	1.601(2)	1.600(2)	1.603(2)
Si-O (Å)	1.614(1)	1.610(2)	1.610(2)	1.609(2)	1.611(1)	1.607(2)
<Si-O> (Å)	1.6092(7)	1.607(1)	1.605(1)	1.605(1)	1.605(1)	1.605(1)
Inter-tetrahedral distances						
Si-Si (Å)	3.05853(8)	3.0193(3)	2.9899(3)	2.9743(3)	2.9666(3)	2.9575(2)
Intra-tetrahedral distances						
O-O (Å)	2.645(1)	2.645(3)	2.650(4)	2.655(3)	2.659(3)	2.664(3)
O-O (Å)	2.631(2)	2.634(3)	2.631(3)	2.625(3)	2.625(3)	2.619(3)
O-O (Å)	2.6171(7)	2.603(1)	2.592(2)	2.586(2)	2.584(1)	2.580(2)
O-O (Å)	2.612(2)	2.618(3)	2.614(4)	2.618(4)	2.614(3)	2.619(4)
Inter-tetrahedral distances						
O-O (Å)	3.331(2)	3.151(3)	3.038(3)	2.982(3)	2.953(3)	2.925(3)
O-O (Å)	3.411(1)	3.260(2)	3.165(3)	3.114(3)	3.092(2)	3.064(2)
Inter-tetrahedral angle						
Si-O-Si (deg)	143.73(7)	139.9(2)	137.2(2)	135.8(2)	135.1(1)	134.2(1)
Intra-tetrahedral angles						
O-Si-O† (deg)	110.52(6)	110.7(1)	111.3(1)	111.6(1)	111.8(1)	112.2(1)
O-Si-O† (deg)	108.81(2)	108.15(4)	107.67(5)	107.31(5)	107.22(4)	106.97(5)
O-Si-O (deg)	108.93(9)	109.4(2)	109.5(2)	109.7(2)	109.6(1)	109.5(2)
O-Si-O (deg)	109.24(8)	109.7(1)	109.5(2)	109.4(2)	109.2(1)	109.1(2)
Quad. Elong.	1.00019	1.00035	1.00067	1.00094	1.00112	1.00139
SiO_4^{4-} Vol. ($Å^3$)	2.138	2.129	2.122	2.119	2.120	2.118

All pressures are reported in kbar unless otherwise noted.
**Parenthesized figures represent esd's of least units cited.*
†*This angle is one of two symmetrically equivalent angles within the tetrahedron.*

Table 5. Unit-cell parameters of quartz at pressure

	a (Å)	c (Å)	V (Å^3)
1 atm	4.916 (1)*	5.4054(4)	113.13(3)
20.7(5) kbar	4.8362(5)	5.3439(4)	108.24(2)
31. (1) kbar	4.785 (3)	5.307 (2)	105.26(8)
37.6(5) kbar	4.7736(7)	5.3010(4)	104.61(2)
48.6(5) kbar	4.739 (1)	5.2785(5)	102.66(3)
55.8(5) kbar	4.7222(5)	5.2673(6)	101.72(3)
61.4(5) kbar	4.7022(3)	5.2561(2)	100.65(3)

* *Parenthesized figures represent esd's of least units cited.*

where c and a are unit-cell parameters and x and z are oxygen coordinates. The values for this angle are essentially equivalent for all three room-pressure data sets (Table 1).

High-pressure structural studies

The changes in the crystal structure observed in our experiments are consistent with the two previous studies (Jorgensen, 1978; d'Amour *et al.*, 1979), but, in addition, our increased precision has allowed us to observe changes not seen in the other two experiments (Table 4). Because we have determined individual Si–O bond distances at pressure to a precision of ±0.002Å, we observe a small change in the average Si–O bond length from 1.6092(7)Å at one atm to 1.605(1)Å at 61.4 kbar (Fig. 1). Both unique Si–O bonds compress at about the same rate (Table 4). We would not have expected Jorgensen's refinements to show this change, as his data are collected only to 28 kbar and his Si–O bond-distance errors are approximately 0.005Å; these errors may partially reflect the effects of Dauphiné twinning on his samples. The d'Amour *et al.* data were collected to high enough pressures (68 kbar) to determine the Si–O bond compression; however, their errors on the Si–O distances were ±0.02Å. The diamond cell used by d'Amour *et al.* contained a sphere of Be (4 cm in diameter) with holes drilled in it so that the crystal could be viewed while under pressure. The spherical shape was used so that a correction for X-ray absorption of the cell would not be necessary; however, the holes in the Be caused large enough deviations from a spherical shape that an absorption correction should have been made (Schulz and d'Amour, personal communication). This problem, combined with the fact that their data were only collected out to 50° 2θ, were responsible for the larger errors. In addition, their crystal/gasket-hole size ratio is small when compared to those normally used in our experiments. When a crystal is too close to the gasket-hole edge, either the incident or diffracted beam can be shielded, causing systematic decreases in the intensities of some reflections.

The compressions of the five shortest non-tetrahedral Si–O distances do not suggest structural movement toward a six-coordinated Si site. The change in the Si···Si distance (Table 4) is nearly linear over the pressure range studied, 3.0585(1)Å at one atm and 2.9575(2)Å at 61.4 kbar. Several pairs of O–O distances decrease more than 0.34Å, or about eleven percent (Fig. 2). At 61.4 kbar these distances, 3.064(2)Å and 2.925(3)Å, are rapidly approaching 2.7Å, the average O–O distance in many silicates at ambient conditions. The common occurrence of this value suggests that there may be a large increase in repulsive energy when oxygens are forced closer than 2.7Å.

The O–O distances within the silicate tetrahedron diverge from the value for a regular tetrahedron as pressure is increased (Table 4). The difference between the longest and shortest distances is 0.033Å at one atm and 0.084Å at 61.4 kbar. This increased tetrahedral distortion is also reflected in the O–Si–O internal tetrahedral angles, which are plotted in Figure 3 along with a dashed line at 109.47°, the internal angle of a regular tetrahedron. The difference between the largest and smallest of the four symmetrically distinct angles is 1.7° at one atm and becomes 5.2° at 61.4 kbar. This increased distortion is consistent with the tetrahedral distortion observed in Jorgensen's (1978) study, but was not observed in the d'Amour *et al.* (1979) work. If distortion of the tetrahedron is measured by quadratic elongation (Robinson *et al.*, 1971) (Table 4), the percent increase gets

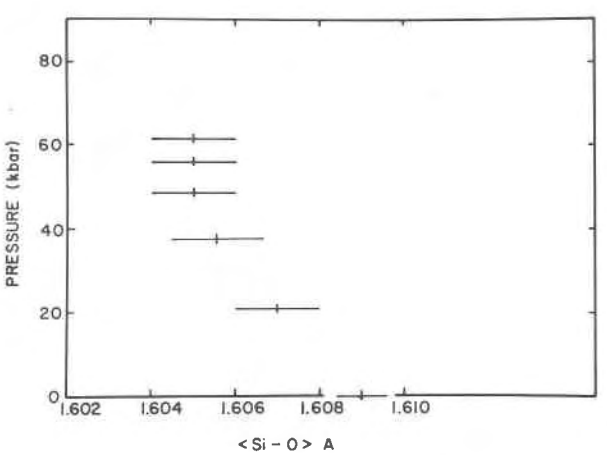

Fig. 1. The change caused by pressure on the average Si–O bond length of quartz.

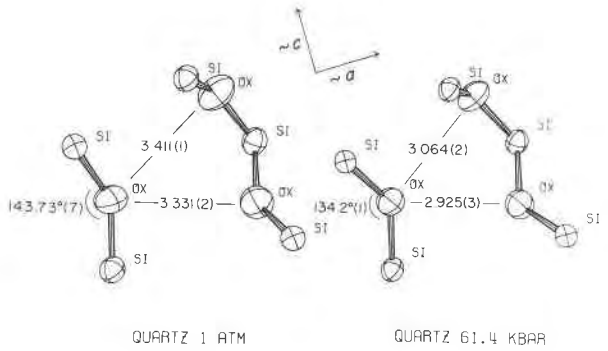

Fig. 2. The effect of pressure on the cavities in the quartz structure. The Si–O–Si angle compresses from 143.73° at 1 atm to 134.2° at 61.4 kbar. The shortening of two long O–O interatomic distances shown in this figure appears to be partially responsible for the difference in compressibilities along the *a* and *c* crystallographic directions.

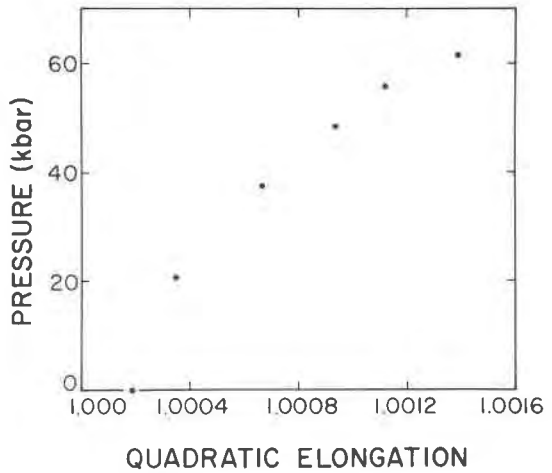

Fig. 4. Increase in tetrahedral distortion with pressure as indicated by quadratic elongation. The curvature of the data indicates that the amount of distortion per kbar is greater at higher prssures than at lower pressures.

larger at higher pressures (Fig. 4), *i.e.*, more distortion takes place between 50 and 60 kbar than between 1 atm and 10 kbar. Because a regular tetrahedron occupies the greatest volume for any tetrahedron of that average size, as it distorts its volume must decrease. Our experiments were not precise enough to show the change in volume due to distortion (Table 4), but we would predict that at higher pressure this volume change would become significant. The structural element responsible for the anomalously high compressibility of quartz is the Si–O–Si interbond angle, which decreases non-linearly by ten degrees over the pressure range from 1 atm to 61 kbar (Figs. 2 and 5). At higher pressures the Si–O–Si angle is responsible for less volume compression; however, the atomic rearrangement that causes the tetrahedron to distort gradually accounts for more compression.

Finally, there is no significant change in the equivalent isotropic temperature factor or orientation of the thermal ellipsoid of Si with pressure; there may be a small decrease in the size of the thermal ellipsoid of O (Table 3). The temperature factor for Si does become more anisotropic as pressure is increased (in our lowest-pressure run), which is consistent with the increased distortion of the tetrahedron.

Unit-cell and elasticity data

Pressure–volume data for quartz (McWhan, 1967; Vaidya *et al.*, 1973; Olinger and Halleck, 1976; Jor-

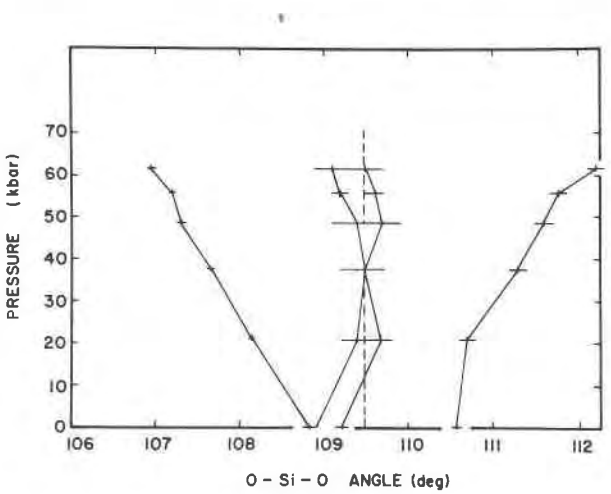

Fig. 3. The pressure dependence of the four unique internal tetrahedral angles (O–Si–O).

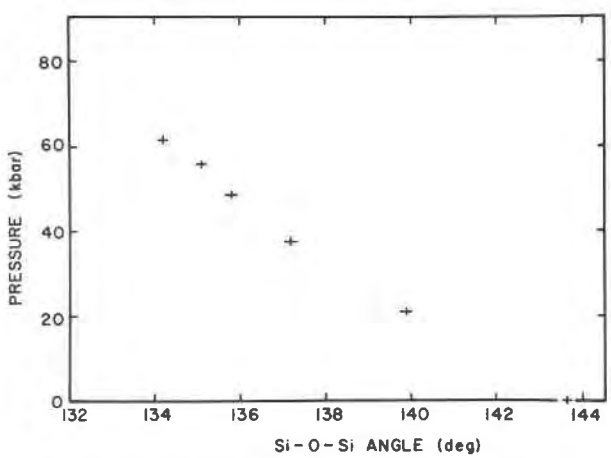

Fig. 5. The pressure dependence of the flexible Si–O–Si angle. The curvature of the data indicates a tapering off of the change in this angle as pressure is increased.

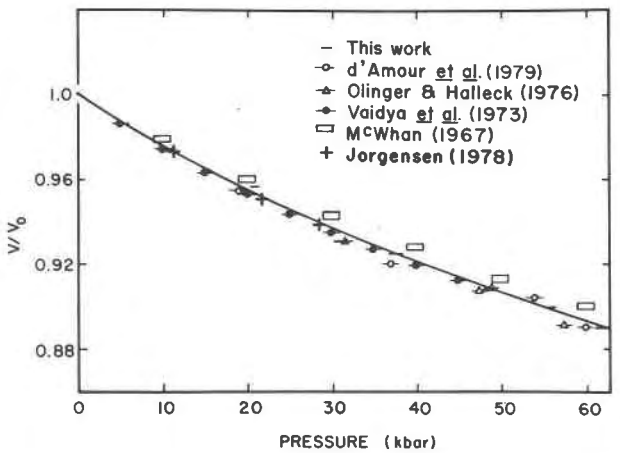

Fig. 6. Unit-cell volume normalized to the ambient unit-cell volume for six compressibility studies of quartz.

gensen, 1978; d'Amour *et al.*, 1979), plotted in Figure 6, show good agreement with the Birch-Murnaghan curve calculated from the ultrasonically determined values of the bulk modulus, K_S, and the pressure derivative of the bulk modulus, K'_S (McSkimin *et al.*, 1965). Isothermal (K_T and K'_T) values have been calculated by fitting the *P–V* data to a Birch-Murnaghan equation of state for each data set, with all pressures converted to Decker (1971) equation of state values to facilitate comparison (Table 6). Values of K_T and K'_T calculated for the McWhan and Vaidya *et al.* studies may differ from the others because both used solid pressure-transmitting media, NaCl and indium metal, respectively. However, calculations of K_T and K'_T and graphs of V/V_0 *vs.* *P* do not give a sufficiently accurate picture of the internal consistency of the data.

In Figure 7 the *c/a* cell-parameter ratio is plotted *vs.* *P*, with all symbols approximately the same size, so errors in data are not represented. For the *c/a* ratio to increase with pressure, the *c* direction must be elastically stiffer than *a*. Using the single-crystal elastic moduli and the pressure derivatives of these moduli from McSkimin *et al.* (1965), the *c/a* ratio can be calculated for high pressures. To make these calculations, lattice parameters are expressed as polynomial expansions, which give notoriously bad lattice-parameter extrapolations to higher pressures. For quartz, such a calculation predicts that with increased pressure the *c/a* ratio reaches a maximum and then decreases at less than 100 kbar. Therefore, on Figure 7 we have used Thurston's (1967) extrapolation formula, which is essentially linear over this pressure range, although it does show a small amount of similar curvature to our data and those of d'Amour *et al.* (1979). The Thurston (solid line) curve diverges from the data at pressures as low as 60 kbar. This discrepancy reflects the need for either second derivatives with respect to pressure of single-crystal elastic moduli, or better extrapolation formulae. The dashed–dotted curve on Figure 7 has been drawn through the data from this study (crosses) and those of Jorgensen (1978) (closed circles), and the dashed curve has been drawn through the d'Amour *et al.* data (open circles) and shows a parallel but systematically offset trend. The excellent agreement at low pressures of our data and the curve predicted by the elastic moduli gives us additional confidence that our experiments were hydrostatic, and that parameters such as bond distances and an-

Table 6. Elasticity data for quartz

Investigator	Technique	K_T (Mbar)*	K'_T
Levien et al.	Single-crystal	0.38 (3)**	6. (2)
d'Amour et al.	Single-crystal	0.365(9)	5.9(4)
Jorgensen	Neutron-powder	0.364(5)	6.3(4)
Olinger and Halleck	Bridgman-anvil	0.38 (1)	5.4(4)
Vaidya et al.	Piston-cylinder	0.347(1)	7.7(1)
McWhan	Bridgman-anvil	0.445(2)	3.6(1)
McSkimin et al.	Ultrasonic	0.371(2)	6.3(3)

*All values for K_T and K_T' determined from pressure-volume data were calculated from a least-squares fit of the P-V data to a Birch-Murnaghan equation of state.

$P = 3/2\ K_T(y^{-7/3} - y^{-5/3})\ [1 - 3/4(4 - K_T')(y^{-2/3} - 1)]$,

$y = V/V_O$.

**Parenthesized figures represent esd's of least units cited.

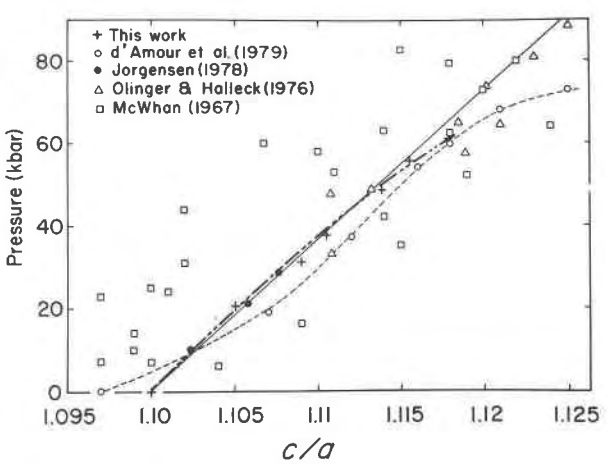

Fig. 7. The *c/a* unit-cell parameter ratio as a function of pressure for five compressibility studies of quartz. The solid line has been determined from Thurston's (1967) extrapolation formula for the McSkimin *et al.* (1965) elastic moduli. The dashed curve is drawn through the d'Amour *et al.* (1979) data, and the dashed–dotted curve is drawn through the data from this study and that of Jorgensen (1978).

gles are consistent with the ultrasonic data. The systematic differences between the high-pressure d'Amour *et al.* unit-cell parameter ratios and ours may have been caused by their crystal being poorly centered (d'Amour, personal communication). The Olinger and Halleck (1976) data (triangles), although showing the proper trend, do not fall along a curve, and the non-hydrostatic McWhan (1967) data (squares) again give the correct general trend, but show a great deal of scatter. Compensating errors in these last two studies gave reasonable values for unit-cell volumes, but only approximate unit-cell edges.

Discussion

Comparison of SiO_2 and GeO_2

As pressure is increased, the geometry of the Si-quartz structure becomes more like the room-pressure Ge-quartz structure. The Si–O–Si angle goes from 143.73° at one atm to 134.2° at 61 kbar, approaching the room-pressure Ge–O–Ge angle of 130° (Smith and Isaacs, 1964). The tetrahedral tilt angle, δ, changes from −16.37° to −23.47°, as compared to the room-pressure Ge-quartz δ of −26.55°. Finally, the O–Si–O angles within the tetrahedron become more like those of the Ge structure under ambient conditions. By 61 kbar the difference between the largest and smallest O–Si–O angles has increased from 1.7° to 5.2°, approaching the 6.8° difference in the one-atm Ge analogue. Therefore, rather than two different structural elements (Si–O–Si angle bending and tetrahedral distortion) controlling the compression of the two crystals, as suggested by Jorgensen (1978), we actually see a continuum. For the quartz structure, substituting Ge for Si appears to have the same effect on the geometry of the structure as increasing the pressure has. Because we see Si–O bond shortening, we would predict some compression of the Ge–O bonds; this was not observed in the Jorgensen study.

Systematic changes in stereochemistry of quartz

Hill and Gibbs (1979) describe an apparent structural interdependence between the Si–O–Si angles and both d(Si–O) and d(Si···Si) in silica polymorphs as well as in silicates. The first relationship, −sec(Si–O–Si) ∝ d(Si–O), suggests that as the Si–O–Si angle decreases the Si–O distance will increase. If true at high pressures, it would predict that Si–O distances might actually increase. In Figure 8 we have plotted the regression line for the room-pressure data (Hill and Gibbs) and the six points (crosses) determined in this study; this correlation does not persist with increased pressure because a coupled decrease in the Si–O–Si angle and the Si–O distance is observed.

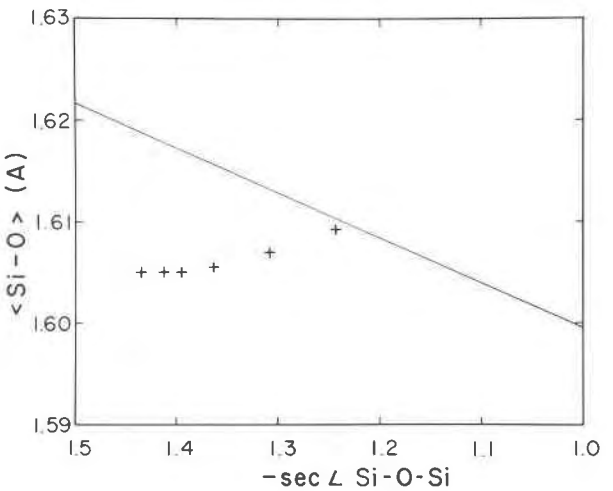

Fig. 8. Si–O bond length as a function of −sec(Si–O–Si) for the silica minerals. The line represents the trend shown in Hill and Gibbs (1979) for the polymorphs measured under ambient conditions; the crosses represent the data for quartz from this study at six pressures, including room pressure. This relationship does not persist at high pressure.

The second relationship in Hill and Gibbs, log sin[(Si–O–Si)/2] ∝ log d(Si···Si), suggests that longer Si···Si separations are associated with wider Si–O–Si angles. In Figure 9 the Hill and Gibbs regression line for this relationship is drawn with our high-pressure data (crosses). This relationship seems to hold better than the first when applied to data other than those obtained under ambient conditions. More structural data are needed on the silica polymorphs to test the validity of this relationship and the importance of non-bonded Si···Si interactions on structural changes under general P–T conditions.

The structural changes that take place during thermal expansion and isothermal compression are not simple inverses. Although the quartz structure is often thought of as compressing and expanding solely through changes in the Si–O–Si angle, as if it behaved like a simple spring, this is not the case. Figures 10 and 11 compare structural changes at elevated temperatures and pressures by plotting unit-cell volume, at P or T divided by the ambient unit-cell volume, against the Si–O–Si angle and the tetrahedral tilt angle, δ, respectively. For these calculations unit-cell data at elevated temperatures were taken from Ackermann and Sorrell (1974), and high-temperature structural data were taken from Young (1962). In Figure 10 there is a break in the slope of the lines

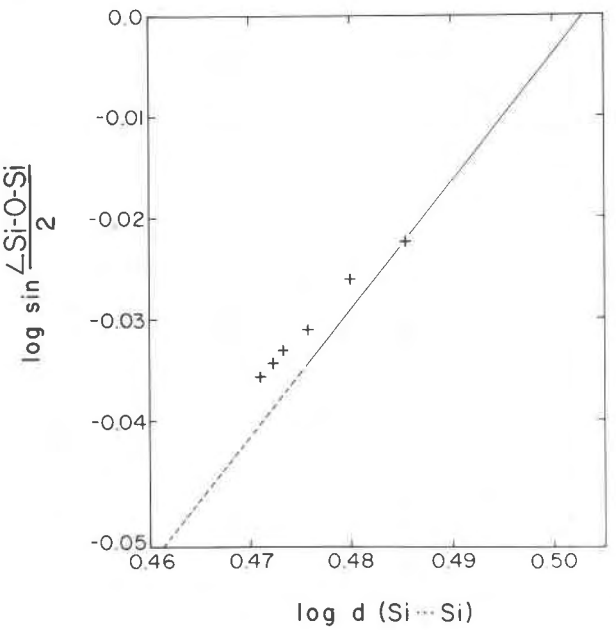

Fig. 9. Plot of log d(Si ··· Si) *vs.* log sin[Si–O–Si)/2] for the silica polymorphs. The line represents the trend shown in Hill and Gibbs (1979) for the silica minerals measured under ambient conditions. The crosses represent the data for quartz from this study, measured at six pressures including room pressure. This relationship may hold for general *P–T* conditions.

connecting the high-temperature and high-pressure points, suggesting that in these two regimes at least partially different structural changes must be responsible for the change of volume. In Figure 11 a hyperbolic curve shows that δ increases rapidly as the α–β transition is approached, but decreases in magnitude more slowly as unit-cell volume is decreased. Although the high-temperature work is not definitive, we conclude that the silicate tetrahedron does not show inverse effects. As temperature is increased, there may be a small increase in distortion (Young); when pressure is increased, tetrahedral distortion increases considerably. It thus appears that the volume increase with temperature is accomplished through changes in the Si–O–Si angle and δ, whereas compression seems to be accomplished by the Si–O–Si angle and increasingly by tetrahedral distortion.

Systematic changes in elasticity of quartz

Several methods have recently been used to investigate the bulk and single-crystal elastic properties of quartz from structural considerations. *Ab initio* calculations, made by modeling quartz from smaller molecules, have determined a bulk modulus for quartz close to the experimental values (O'Keeffe *et al.*, 1980). We have investigated how atomic rearrangements reflect single-crystal elastic properties. The structural reason for the changing c/a cell-parameter ratio (Fig. 7) can be seen in Figure 2, on which we have drawn approximate crystallographic axes. One of the rapidly changing O–O distances is nearly parallel to a; the other is approximately 45° between a and c. Hence there is more compression of these distances in the a direction than in the c direction, explaining the stiffer elastic nature of c.

The errors on the bulk modulus, K_T, and the pressure derivative of the bulk modulus, K'_T, listed in Table 6, are based on the assumption that the scatter of the data from the curve being fit accurately represents the errors on the pressure and volume of each point; this is often not the case (Bass *et al.*, 1979). When the errors associated with each point of our quartz data are included in the analysis, K_T and K'_T are very poorly constrained. Therefore, Bass *et al.* have fixed the value of K_T equivalent to the Reuss bound, calculated from the acoustically determined single-crystal elastic moduli (McSkimin *et al.*, 1965) and corrected for the difference between isothermal and adiabatic experiments. Using a weighted fit of our data, holding $K_T = 0.371(2)$ Mbar, they calculate $K'_T = 6.2(1)$, in excellent agreement with McSkimin *et al.*'s acoustic value of 6.3(3).

Using any two bulk elastic moduli, the elastic character of an isotropic material (an ideal polycrystal) can be described. A common pair of such moduli are Young's modulus, E, and Poisson's ratio,

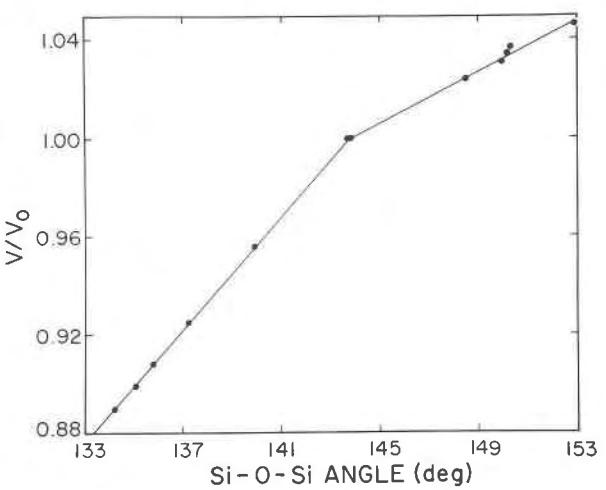

Fig. 10. The Si–O–Si angle of quartz as a function of unit-cell volume at temperature or pressure normalized to room-pressure–temperature volume. The break in slope at the room-temperature–pressure point suggests that different structural changes cause the volume change for increased temperature or pressure.

σ, which describe the lengthening and necking of a rod under tensile stress. Poisson's ratio can be written in terms of K, the bulk modulus, and μ, the shear modulus: $\sigma = (3K - 2\mu)/2(3K + \mu)$. The Voigt bound of K can be expressed as 1/9[a + 2b] where, for the case of quartz, $a = 2c_{11} + c_{33}$ and $b = 2c_{13} + c_{12}$ (c_{ij}'s are single-crystal elastic moduli); μ can be written as 1/15[a − b + 3c] where a and b are as above, and $c = 2c_{44} + c_{66}$. Therefore $\sigma = [a + 4b - 2c]/[4a + 6b + 2c]$. The value of σ for quartz is 0.056, yet for most minerals $\sigma \simeq 0.25$. To understand why σ commonly equals 0.25, we assumed $\sigma = 0.25$ and solved this equation. The result is that b equals c. Therefore, for most minerals the sum of the pure-shear elastic moduli (c) is approximately equal to the sum of the off-diagonal shear moduli (b). In quartz the ratio of b/c is 0.2 instead of 1.0 (McSkimin *et al.*, 1965).

Single-crystal elastic moduli each describe the structural deformation that takes place when a given stress is applied to a crystal. The pure-shear elastic moduli (c_{44} and c_{66}) indicate the amount of shear stress required to produce a unit shear strain in the *a*–*c* plane (c_{44}) and the a_1–a_2 plane (c_{66}). One of the off-diagonal elastic moduli, c_{13}, describes the stress induced in the *c* direction due to a strain parallel to *a*; the other, c_{12}, describes the similar coupling between a_1 and the direction perpendicular to a_1 and *c*. When a coil spring is shortened parallel to its axis, very little stress is induced in a direction perpendicular to the axis. Exactly such a change can be easily accommodated by the quartz structure which is comprised of tetrahedra repeated along threefold screw axes parallel to *c* (Fig. 12). When a length change occurs parallel to *c*, the small value of c_{13} suggests that there is a small concomitant change in *a*. In addition, if a length change occurs parallel to a_1, a small change in the direction perpendicular to a_1 and *c* results. This behavior dominates the elastic behavior of a polycrystal. We therefore believe the small value for Poisson's ratio is caused by the easily expanding and contracting spirals of tetrahedra which behave like coiled springs. Thus for this relatively simple structure the shear moduli can be rationalized from structural considerations. Although this work provides only a beginning, we hope that additional detailed studies of crystal structures at high pressures, and the relationships of structural changes to the single-crystal elastic properties of the same materials, will eventually lead to general empirical relationships that may help us to predict elastic properties of minerals as they exist within the Earth.

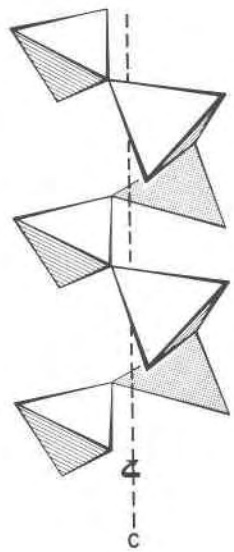

Fig. 12. Spirals of silicate tetrahedra parallel to *c*. These easily expanding and contracting spirals behave like coiled springs and are, therefore, responsible for the low value of Poisson's ratio in quartz.

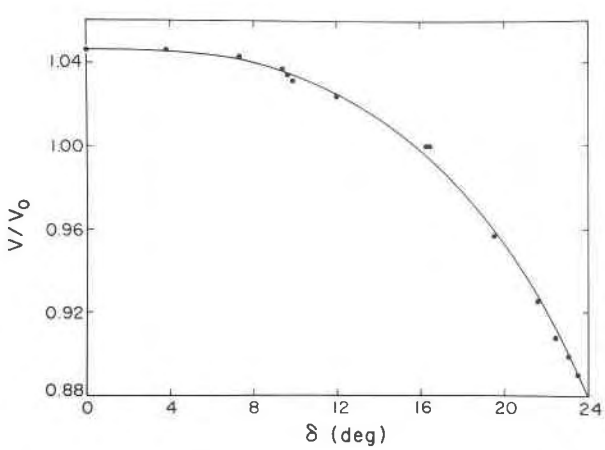

Fig. 11. The tetrahedral tilt parameter for quartz, δ, as a function of unit-cell volume at temperature or pressure normalized to the room-temperature–pressure volume. The hyperbolic shape of this curve suggests that tetrahedral tilting is important to the change in unit-cell volume as the α–β transition is approached but has less effect as unit-cell volume decreases.

Acknowledgments

We thank J. D. Bass for developing the program to calculate the elastic parameters, and J. D. Bass and R. C. Liebermann for helpful discussions about the elasticity sections of this paper. This research was supported by NSF grant EAR77-13042. The first author also gratefully acknowledges a pre-doctoral fellowship awarded to her by the American Association of University Women Educational Foundation.

References

Ackermann, R. J. and C. A. Sorrell (1974) Thermal expansion and the high–low transformation in quartz. I. High-temperature X-ray studies. *J. Appl. Crystallogr., 7,* 461–467.

Adams, L. H. and E. D. Williamson (1923) Compressibility of minerals and rocks at high pressure. *J. Franklin Inst., 195,* 475–529.

Barnett, J. D., S. Block and G. J. Piermarini (1973) An optical fluorescence system for quantitative pressure measurement in the diamond-anvil cell. *Rev. Sci. Instrum., 44,* 1–9.

Bass, J. D., R. C. Liebermann, D. J. Weidner and S. J. Finch (1979) Elasticity data from acoustic and volume compression experiments (abstr.). *Trans. Am. Geophys. Union, 60,* 386.

Bridgman, P. W. (1925) Linear compressibility of fourteen natural crystals. *Am. J. Sci., 10,* 483–498.

——— (1928) The linear compressibility of thirteen natural crystals. *Am. J. Sci., 15,* 287–296.

——— (1948a) The compression of 39 substances to 100,000 kg/cm^2. *Proc. Am. Acad. Arts Sci., 76,* 55–70.

——— (1948b) Rough compressions of 177 substances to 40,000 kg/cm^2. *Proc. Am. Acad. Arts Sci., 76,* 71–87.

——— (1949) Linear compression to 30,000 kg/cm^2, including relatively incompressible substances. *Proc. Am. Acad. Arts Sci., 77,* 189–234.

d'Amour, H., W. Denner and H. Schulz (1979) Structure determination of α-quartz up to 68 × 10^8 Pa. *Acta Crystallogr., B35,* 550–555.

Decker, D. L. (1971) High-pressure equation of state for NaCl, KCl, and CsCl. *J. Appl. Phys., 42,* 3239–3244.

Finger, L. W. and E. Prince (1975) A system of Fortran IV computer programs for crystal structure computations. *U. S. Natl. Bur. Stand. Tech. Note 854.*

——— and H. King (1978) A revised method of operation of the single-crystal diamond cell and the refinement of the structure of NaCl at 32 kbar. *Am. Mineral., 63,* 337–342.

Grimm, H. and B. Dorner (1975) On the mechanism of the α–β phase transformation of quartz. *J. Phys. Chem. Solids, 36,* 407–413.

Hamilton, W. C. (1974) Tests for statistical significance. In J. A. Ibers and W. C. Hamilton, Eds., *International Tables for X-Ray Crystallography,* Vol. IV, p. 285–310. Kynoch Press, Birmingham, England.

Hazen, R. M. and L. W. Finger (1977) Modifications in high-pressure single-crystal diamond-cell techniques. *Carnegie Inst. Wash. Year Book, 76,* 655–656.

Hill, R. J. and G. V. Gibbs (1979) Variation in d(T–O), d(T···T) and <TOT in silica and silicate minerals, phosphates and aluminates. *Acta Crystallogr., B35,* 25–30.

Jorgensen, J. D. (1978) Compression mechanisms in α-quartz structures—SiO_2 and GeO_2. *J. Appl. Phys., 49,* 5473–5478.

King, H. E., Jr. (1979) *Phase Transitions in FeS at High-Temperatures and High-Pressures.* Ph.D. Thesis, State University of New York, Stony Brook, New York.

——— and L. W. Finger (1979) Diffracted beam crystal centering and its application to high-pressure crystallography. *J. Appl. Crystallogr., 12,* 374–378.

Le Page, Y. and G. Donnay (1976) Refinement of the crystal structure of low-quartz. *Acta Crystallogr., B32,* 2456–2459.

McSkimin, H. J., P. Andreatch, Jr. and R. N. Thurston (1965) Elastic moduli of quartz versus hydrostatic pressure at 25° and −195.8°C. *J. Appl. Phys., 36,* 1624–1632.

McWhan, D. B. (1967) Linear compression of α-quartz to 150 kbar. *J. Appl. Phys., 38,* 347–352.

Merrill, L. and W. A. Bassett (1974) Miniature diamond anvil pressure cell for single crystal X-ray diffraction studies. *Rev. Sci. Instrum., 45,* 290–294.

O'Keefe, M., M. D. Newton and G. V. Gibbs (1980) Ab initio calculation of interatomic force constants in $H_6Si_2O_7$ and the bulk modulus of α-quartz and α-cristobalite. *Phys. Chem. Mineral.,* in press.

Olinger, B. and P. M. Halleck (1976) The compression of α quartz. *J. Geophys. Res., 81,* 5711–5714.

Piermarini, G. J., S. Block and J. D. Barnett (1973) Hydrostatic limits in liquids and solids to 100 kbar. *J. Appl. Phys., 44,* 5377–5382.

———, ———, ——— and R. A. Forman (1975) Calibration of the pressure dependence of the R_1 ruby fluorescence line to 195 kbar. *J. Appl. Phys., 46,* 2774–2780.

Robinson, K., G. V. Gibbs and P. H. Ribbe (1971) Quadratic elongation: a quantitative measure of distortion in coordination polyhedra. *Science, 172,* 567–570.

Smith, G. S. and L. E. Alexander (1963) Refinement of the atomic parameters of α-quartz. *Acta Crystallogr., 16,* 462–471.

——— and P. B. Isaacs (1964) The crystal structure of quartz-like GeO_2. *Acta Crystallogr., 17,* 842–856.

Thurston, R. N. (1967) Calculation of lattice-parameter changes with hydrostatic pressure from third-order elastic constants. *J. Acoust. Soc. Am., 41,* 1093–1111.

Vaidya, S. N., S. Bailey, T. Pasternack and G. C. Kennedy (1973) Compressibility of fifteen minerals to 45 kilobars. *J. Geophys. Res., 78,* 6893–6898.

Young, R. A. (1962) Mechanism of phase transition in quartz. *AFOSR-2569 (Final Report, Project No. A-447) Engineering Experimental Station, Georgia Institute of Technology.*

——— and B. Post (1962) Electron density and thermal effects in alpha quartz. *Acta Crystallogr., 15,* 337–346.

Zachariasen, W. H. (1963) The secondary extinction correction. *Acta Crystallogr., 16,* 1139–1144.

——— (1967) A general theory of X-ray diffraction in crystals. *Acta Crystallogr., 23,* 558–564.

——— and H. A. Plettinger (1965) Extinction in quartz. *Acta Crystallogr., 18,* 710–714.

Manuscript received, May 31, 1979;
accepted for publication, April 18, 1980.